

## A STUDY OF GIANT PULSES FROM PSR J1824–2452A

H. S. KNIGHT<sup>\*†</sup>, M. BAILES

Centre for Astrophysics and Supercomputing, Swinburne University of Technology, P.O. Box 218, Hawthorn VIC 3122, Australia

R. N. MANCHESTER

Australia Telescope National Facility, CSIRO, P.O. Box 76, Epping NSW 1710, Australia

AND

S. M. ORD

School of Physics, University of Sydney, NSW 2006, Australia

*To be submitted to ApJ*

### ABSTRACT

We have searched for microsecond bursts of emission from millisecond pulsars in the globular cluster M28 using the Parkes radio telescope. We detected a total of 27 giant pulses from the known emitter PSR J1824–2452A. At wavelengths around 20 cm the giant pulses are scatter-broadened to widths of around  $2\ \mu\text{s}$  and follow power-law statistics. The pulses occur in two narrow phase-windows which correlate in phase with X-ray emission and trail the peaks of the integrated radio pulse-components. Notably, the integrated radio emission at these phase windows has a steeper spectral index than other emission. The giant pulses exhibit a high degree of polarization, with many being 100% elliptically polarized. Their position angles appear random. Although the integrated emission of PSR J1824–2452A is relatively stable for the frequencies and bandwidths observed, the intensities of individual giant pulses vary considerably across our bands. Two pulses were detected at both 2700 and 3500 MHz. The narrower of the two pulses is 20 ns wide at 3500 MHz. At 2700 MHz this pulse has an inferred brightness temperature at maximum of  $5 \times 10^{37}$  K. Our observations suggest the giant pulses of PSR J1824–2452A are generated in the same part of the magnetosphere as X-ray emission through a different emission process to that of ordinary pulses.

*Subject headings:* pulsars:general — pulsars:individual (PSR B1821–24, PSR J1824–2452, PSR J1824–2452A)

### 1. INTRODUCTION

The Crab pulsar was discovered through the observation of a series of strong bursts of radio emission (Staelin & Reifenstein 1968). The sampling interval of this search was about 18 times the 33 ms pulse period, so if all of its pulses had been equal to the average pulse it would have been rendered invisible. Instead, the pulses followed power-law statistics, and so some pulses with energies many times stronger than the average pulse-energy were detected. These giant pulses (GPs) are composed of  $\lesssim 2$  ns ultra-bright shots (Hankins et al. 2003) that can occur in emission envelopes that are as long as  $\sim 100\ \mu\text{s}$  (Sallmen et al. 1999; Knight 2006). Propagative effects have a frequency-dependent nature. As the spacing and number of shots are frequency independent, the observed multiplicity of components is due to the emission mechanism itself (Sallmen et al. 1999).

The GPs are most readily found in the main-pulse and inter-pulse radio components, which correlate in phase with the optical, X-ray, and  $\gamma$ -ray pulse peaks (Lundgren et al. 1995). Other radio pulse-components do not have associated high-energy emission, but some GPs are seen at their phases (Jessner et al. 2005).

The individual nano-shots of GPs from the Crab pulsar have a high degree of circular polarization and come in both orientations (Hankins et al. 2003). The distribu-

tion in degree of circular polarization of unresolved GPs can be accurately modelled by assuming superpositions of many ( $\sim 100$ ) nano-pulses that are 100% circularly polarized (Popov et al. 2006).

The millisecond pulsars B1937+21, J1824–2452A, J1823–3021A, J0218+4232, and B1957+20 have also been shown to emit short-timescale pulses with inferred brightness-temperatures ( $T_B$ ) that are very high (Cognard et al. 1996; Romani & Johnston 2001; Knight et al. 2005, 2006; Knight 2006). Although many of these ultra-bright pulses are weaker in pulse-energy terms than the average pulse (see, e.g. Soglasnov et al. 2004), they can be defined as GPs through a number of other criteria. These are that they are always unresolved on microsecond timescales, occur in narrow phase-windows that align with X-ray emission, and that their energies follow power-law statistics. Unlike the GPs of the Crab pulsar, the GPs from the millisecond pulsars do not occur at all phases where integrated emission is seen, and do not contribute markedly to the integrated emission profile. For PSR B1937+21 the GPs occur at the extreme trailing edges of the two integrated emission components. Soglasnov et al. (2004) found that the GPs from PSR B1937+21 usually consist of single  $\sim 16$  ns shots, but also presented a pulse with structure over hundreds of nanoseconds. Popov et al. (2004) found that at 600 MHz the GPs from PSR B1937+21 are  $< 10\%$  linearly polarized and highly circularly polarized.

PSR J1824–2452A is an isolated millisecond pulsar

<sup>\*</sup>Affiliated with the Australia Telescope National Facility, CSIRO

<sup>†</sup>Email: hknight@astro.swin.edu.au

with a period of  $P = 3.054$  ms. It is located 5.6 kpc from the Sun in the globular cluster M28 (Lyne et al. 1987; Harris 1996). Acceleration in the potential of its host cluster means the period derivative ( $\dot{P}$ ) contribution from spin down is not directly observable, and consequently other derived parameters are not known with certainty. However, indirect evidence exists that the large  $P$  observed is indicative of the true value — PSR J1824–2452A glitches (Cognard & Backer 2004), emits GPs, emits strong X-ray pulses (Rots et al. 1998), and has a large second period derivative ( $\ddot{P}$ ) (Cognard et al. 1996). If the observed  $\dot{P}$  is similar to the intrinsic value, then PSR J1824–2452A is around 30 Myr old and it and PSR J1823–3021A are the youngest millisecond pulsars known. This assumption also means that PSRs J1824–2452A and B1937+21 have inferred magnetic fields at their light cylinders ( $B_{LC} \propto P^{-2.5} \dot{P}^{0.5}$ ) and spin-down luminosities ( $\dot{E} \propto P^{-3} \dot{P}$ ) that are the highest of all millisecond pulsars.

Romani & Johnston (2001) (hereafter RJ01) discovered GPs at a center frequency ( $\nu$ ) of 1520 MHz from PSR J1824–2452A with energies as low as 30 times the mean pulse-energy,  $\langle E \rangle$ . Use of a hardware filter-bank on a high dispersion measure source ( $\sim 120$  pc cm $^{-3}$ ) limited their effective time resolution to 200  $\mu$ s and they were unable to resolve the pulses. Six of the eight brightest pulse detections fell within a single phase-window, which slightly trailed one of the three pulse components. To date, it has been unclear how narrow the GPs from PSR J1824–2452A are, and whether they have substructure like GPs from the Crab pulsar.

In this paper we use a baseband recorder to achieve much finer time resolution than RJ01 in an attempt to uncover and study a larger population of GPs emanating from millisecond pulsars in M28. We resolve the GPs from PSR J1824–2452A, better quantify their phase and energy distributions, and perform a polarimetric analysis.

## 2. OBSERVATIONS AND DATA ANALYSIS

Observations were taken using the Parkes 64-m radio telescope between 2003 February and 2004 December. All data were taken using the Caltech-Parkes-Swinburne-Recorder Mark II (CPSR2) (Bailes 2003). This is a baseband recorder that two-bit samples one or two dual-polarization 64 MHz bands at the Nyquist rate. Coherent dedispersion (Hankins & Rickett 1975; Stairs 1998; van Straten 2003) can be performed on the input stream to remove the cold-plasma dispersion of the interstellar medium (ISM) to give an effective sampling rate of 7.8125 ns per 64 MHz band. However, it is more advantageous with respect to interference removal and computing requirements to form a “coherent filter-bank” that gives enhanced frequency resolution at the cost of reduced time resolution. In the initial searches a 256-channel filter bank was formed at a DM of 119.868 pc cm $^{-3}$  and searched for bursts of emission at sampling times of 4 – 128  $\mu$ s. Initial searches were carried out over a DM range of 0.1 pc cm $^{-3}$ , but later searches used increased ranges of up to 6.0 pc cm $^{-3}$ . Within these ranges, coherent dedispersion and channel-summing were repeatedly performed so as to ensure dispersive smearing across the entire band was always less than 4  $\mu$ s.

PSR J1824–2452F, which has a DM of 123.8 pc cm $^{-3}$  (Ransom et al. 2005), is an example of a pulsar whose DM meant that these searches probably did not probe its emission effectively. Data were searched with a variety of algorithms, and in general data files without candidates were deleted. Subsequently, the remaining data files were re-dedispersed multiple times and searched at time resolutions down to 0.5  $\mu$ s so as to remove dispersive smearing for DMs between 116.9 and 124.9 pc cm $^{-3}$ . Table 1 summarizes the data taken. Columns 1 and 2 respectively show the observation date and receiver used. All receivers used have two orthogonal linear probes. The center frequency observed and system equivalent flux density (SEFD) for the on-source observations are shown in columns 3 and 4 respectively. Columns 5 and 6 show the total duration of the initial and secondary searches respectively, and column 7 shows the flux density of PSR J1824–2452A. The criteria for a detection leading to human scrutiny in the secondary search was two consecutive samples adding to give a spike 13 times the RMS. The detection threshold for 4  $\mu$ s sampling is shown in column 8 in absolute terms, and in column 9 in terms of the mean pulse-energy of PSR J1824–2452A. The radiometer equation (see, e.g. Edwards 2001) dictates that the minimum energy detectable varies as  $t_{\text{samp}}^{0.5}$ , where  $t_{\text{samp}}$  is the sampling time used. Therefore the threshold for the later searches, which had shorter sampling times, was lower for unresolved pulses.

## 3. SEARCH RESULTS

At 1341 – 1720 MHz (hereafter 20 cm) 25 pulses were detected and confirmed to be associated with PSR J1824–2452A by virtue of occurring at its DM. Of these, 21 were seen in 2003 and 4 were seen in 2004. In addition, two pulses from PSR J1824–2452A were observed at 2700 MHz. Counterparts to these two pulses were revealed in 3500 MHz data upon further inspection. No pulses were found from other sources in the cluster. PSR J1824–2452C is  $\sim 170$   $\mu$ Jy at 1950 MHz and is one of the brightest of the other pulsars (Ransom et al. 2005; Ransom 2006, priv. comm.). If a spectral index ( $\alpha_{\text{spec}}$ ) of  $-1.9$  is assumed for this 4.159 ms pulsar, its average flux-density at 1341 MHz is 350  $\mu$ Jy and its average pulse energy is 1.4 Jy  $\mu$ s. Therefore, our 91 Jy  $\mu$ s threshold in Table 1 at 1341 MHz corresponds to a threshold of  $60 \langle E \rangle$ . Although this is not particularly constraining given the paucity of such strong pulses emitted by the known GP emitters PSRs J0218+4232 and B1957+20 (Knight et al. 2006), it can be said that PSR J1824–2452C is unlikely to emit GPs at high rate.

### 3.1. Phases

The phases of the pulses detected from PSR J1824–2452A in 2003 February and 2003 April are shown in Figure 1. We follow the numbering convention of Backer & Sallmen (1997) and denote the leading steep-spectrum component at phase 0.35 as P1, and the trailing two components as P2 and P3 respectively. The pulse population at phase 0.37 occurs over 0.006 periods (18  $\mu$ s) and trails the center of the P1 component by around 0.02 periods. Both of the pulses seen at 2700 MHz also come from the vicinity of this window. Despite these two pulse detections at 2700 MHz, phase-coherent summation of  $3 \times 10^6$

pulses was not enough to provide a detection of the accompanying P1 component. If PSR J1824–2452A did not emit P2 pulses, at high frequency it would be more readily detected through individual GPs than through its integrated emission.

The main-pulse GPs of PSR B1937+21 occur over a window of similar width to that of PSR J1824–2452A — 0.007 periods (Soglasnov et al. 2004). The GP emission zones of PSR J1824–2452A have nearly equal phases to the peaks of the X-ray pulses. We consider that any misalignment is close to the error in the phase determination. The 1341 MHz pulse detected at phase 0.92 was  $21\langle E \rangle$  and well above the detection threshold. Another pulse with a similar phase was detected in 2004 November, and RJ01 also detected a pulse here. Therefore, there is definitely a secondary GP population around phase 0.92.

### 3.2. Energies

At a sampling interval of  $12\mu\text{s}$  all visible 20 cm pulses had intensities above 50% of the peak intensity for just one or two samples. This sampling interval was therefore used to determine the FWHM energies of these pulses. The most energetic pulse was  $91\langle E \rangle$  and the weakest was  $8.4\langle E \rangle$ . At high frequency our estimates are uncertain due to the poor signal to noise ratio of the integrated profile, but the two pulses seen at 2700 MHz (hereafter pulses 1 and 2) had energies around 260 and  $114\langle E \rangle$  respectively. Their counterparts at 3500 MHz were discovered by analysing the profiles of the pulses the GPs occurred in, and were  $104$  and  $105\langle E \rangle$  respectively.

At  $\nu \geq 2700$  MHz only one component is visible in the integrated profile of PSR J1824–2452A, and this is taken to be the P2 component. No GPs occur at the phase of this component, and so its average energy may not be related to the GP energies. The average P1 energy,  $\langle E_{P1} \rangle$ , may be a better measure of how strong a GP is. At 1341 MHz 36% and 49% of the total radio flux-density ( $S$ ) of PSR J1824–2452A is emitted in the P1 and P2 components respectively. Extrapolation can be performed using the  $\alpha_{\text{spec (P1)}} = -3.1$  and  $\alpha_{\text{spec (P2)}} = -1.4$  spectral indices found by Foster et al. (1991). At 2700 MHz  $S_{P2}/S_{P1}$  is therefore larger than at 1341 MHz by a factor of around  $(2700/1341)^{3.1-1.4} = 3.3$ . The  $260\langle E_{P2} \rangle$  pulse seen at 2700 MHz is equivalent to a  $1200\langle E_{P1} \rangle$  pulse at 1341 MHz. This is a  $\gtrsim 400\langle E \rangle$  pulse, which is far stronger than any of the pulses seen at 20 cm. Therefore, the GP must be stronger relative to the average pulse at high frequency than at low frequency. This means that GPs are probably strong only over moderate bandwidths. Further evidence supporting this hypothesis is the fact that the GP had a steep spectral index of  $-5.4$ .

### 3.3. Rates

A probability distribution for pulse energies following power-law statistics can be expressed in the form:

$$P(E > E_0) = KE_0^{-\alpha}, \quad (1)$$

where  $E_0$  is measured in terms of the mean pulse energy. Integration gives the fraction of radio energy emitted in the form of GPs of energies greater than  $E_0$ ,

$$S_{\text{GP}}(E > E_0) = \frac{K\alpha}{\alpha - 1} E_0^{1-\alpha}. \quad (2)$$

A cumulative probability distribution for the 20 cm pulses is shown in Figure 2. Exclusion of the 3 most energetic and 3 least energetic pulses yields a best-fit power-law with  $K = 2.5 \times 10^{-4}$  and  $\alpha = 1.6$ . Both the plot and the energy thresholds of Table 1 indicate pulses below  $22\langle E \rangle$  have been missed. Exclusion of the 8 least energetic pulses gives a similar fit but exclusion of 15 low-energy pulses gives an alternative fit with  $\alpha = 2.3$ . Power-law indices in the range 1.4 – 2.5 have been fitted for pulsars that emit GPs (Knight et al. 2006), and so both fits are plausible. By comparison RJ01 suggested  $\alpha$  is in the range of 3 – 5. This range of values is inconsistent with our data.

Assuming the original  $\alpha = 1.6$  fit,  $P(E > 28\langle E \rangle) = 1.3 \times 10^{-6}$ , which is similar to the value of  $\sim 8.5 \times 10^{-7}$  of RJ01. We find that PSR J1824–2452A emits GPs with total energies of  $20\langle E \rangle$  at about 0.5 and 3 times the rates of PSRs B1937+21 and J0218+4232 respectively (Soglasnov et al. 2004; Knight et al. 2005).

The overall contribution of GPs to the pulse profile of PSR J1824–2452A is difficult to ascertain because they lie in a region where ordinary emission occurs. Analysis of the pulse profile suggests that at 1341 MHz the integrated flux-density averages  $\sim 5$  mJy over the GP phases. The flux-density integrated over this window makes up  $\sim 3\%$  of the flux-density integrated over the entire profile. For GP emission contributing 100%, 10%, and 1% of the total flux-density over the GP phases, equation (2) gives low-energy cut-offs of  $1.7 \times 10^{-3}$ ,  $8.8 \times 10^{-2}$ , and  $4.6\langle E \rangle$  respectively. Soglasnov et al. (2004) found that the GP distribution of PSR B1937+21 probably extends to energies of  $0.016 - 0.032\langle E \rangle$ . If a similar cut-off occurs for PSR J1824–2452A then a 20 – 30% increase in flux density would be expected at the phase of the GPs. Such a bump may be detectable by 100 m class telescopes.

## 4. PULSE WIDTHS

Pulse profiles binned at 750 ns gave full widths at half-maximum (FWHM) for the 20 cm pulses of between 750 ns and  $6.0\mu\text{s}$ . The FWHM of the strongest 2003 pulses were 2.2 and  $1.1\mu\text{s}$  at 1341 and 1720 MHz respectively. Although these widths imply a flatter frequency dependence than the  $\nu^{-4.4}$  spectrum of Kolmogorov-spectrum scattering (Rickett 1996), we think that more pulses need to be studied to make definite conclusions. A 1341 MHz pulse representative of other 2003 pulses with regard to typical width and shape is shown in Figure 3, along with several pulses observed in 2004. Emission above 30% of the peak is seen at long delays for all 2004 pulses but not for any 2003 pulses. The exponential decay time of the scattering tail therefore substantially changes on  $\sim 1$  yr timescales.

The high-frequency observations taken in 2003 December used two bands separated by 800 MHz. By aligning pulses from the two bands we obtained a DM of  $119.8688 \pm 0.0002$  for this epoch, sufficiently accurate to allow dedispersion to remove all dispersive effects of a cold ISM to the 7.8125 ns Nyquist sampling-rate for each band. Fully dedispersed profiles of PSR J1824–2452A are shown in Figure 4. Pulse 1 appears to be intrinsically broader than pulse 2 and at 2700 MHz has more unresolved structure occurring hundreds of nanoseconds after the main pulse. A  $\nu^{-4.4}$  extrapolation of the  $1.1\mu\text{s}$  FWHM at 1720 MHz predicts widths of 150 and 48 ns at

2700 and 3500 MHz respectively. Given that the structure disappears at 3500 MHz we consider that it is probably a manifestation of scattering in the ISM. Alternatively it could be narrow-band, or just receiver noise.

At high frequencies the pulse width does not seem to scale with frequency — pulse 1 at 3500 MHz is broader than either pulse at 2700 MHz. We may therefore be resolving the pulse envelopes. If this is true, moderately enhanced time resolution could reveal whether the emission consists of short strong bursts interspersed by intervals where there is little or no emission. Our observations provide no evidence that pulse 2 is anything other than a single coherent shot. It has a FWHM of 20 ns at 3500 MHz, which is similar to the  $\sim 15$  ns inferred for the GPs of PSR B1937+21 (Soglasnov et al. 2004). The pulse reaches 2300 Jy and therefore has an inferred brightness temperature at maximum of  $5 \times 10^{37}$  K, which is higher than the nano-pulses directly observed from the Crab pulsar (Hankins et al. 2003). However, simulations of the ISM response of GPs from PSR B1937+21 by Soglasnov et al. indicate that its GPs can reach  $T_B \sim 5 \times 10^{39}$  K, which is much brighter.

### 5. POLARIMETRY

The 2003 April GPs and integrated profiles were calibrated using the PSRCHIVE software library (Hotan et al. 2004) using a similar methodology to Ord et al. (2004). The 1341 and 1720 MHz polarimetric profiles of PSR J1824–2452A are shown in Figure 5. At 1341 MHz the high flux-density portions of the P1 and P2 pulse components are respectively 72% and 96% linearly polarized. We detect no circular polarization in any component and no polarization at all in the P3 component. The position angle swing between the center of the P1 component and the peak of the P2 component is  $48^\circ$  at 1341 MHz, which is similar to that presented by other authors (Backer & Sallmen 1997; Stairs et al. 1999; Ord et al. 2004). We find no evidence in our data for the mode-changing described by Backer & Sallmen (1997). The P1b component of the 1720 MHz profile is reduced in intensity when compared to the 1341 MHz profile. The peak flux-density in this phase zone scales as  $\nu^{-4.4}$ , whereas the flux-densities of the earlier P1 (P1a) and the P2 peaks scale as  $\nu^{-2.8}$  and  $\nu^{-1.9}$  respectively. (Kinkhabwala & Thorsett 2000) found that on average GPs from PSR B1937+21 have spectral indices steeper than the integrated emission. However, this cannot be the case for the GPs of PSR J1824–2452A — a power-law steeper than  $\nu^{-4.4}$  would have precluded our detections of GPs above 2 GHz.

By maximizing the linear polarization of the mean pulse-profile we fit a rotation measure (RM) of  $78.5 \pm 0.9 \text{ rad m}^{-2}$ . The RM of  $1 \pm 12 \text{ rad m}^{-2}$  published by Rand & Lyne (1994) is wrong. Polarization properties of 13 GPs are summarized in Table 2. The first three rows of data respectively show the linear, circular, and total polarization fractions. The last row shows the ratio of circular to linear polarization. Minimum, mean, and maximum fractions for each of these quantities are shown in columns 2, 3, and 4 respectively. The GPs have both signs of circular polarization. Hankins et al. (2003) and Popov et al. (2004, 2006) studied the polarization of GPs of PSR B1937+21 and the Crab pulsar, but neither group reported significant linear polarization. By

contrast, the GPs of PSR J1824–2452A are highly elliptically polarized. Some are even 100% linearly polarized. The position angles of the GPs appear to be random, as shown in Figure 6. This could be due to a propagation effect, or it could be intrinsic to the emission mechanism of the GPs. In the later case, it would mean that the preferred axis of the emission region varies — i.e. a strong local field temporarily dominates over the global dipole. This could be indicative of small-scale plasma turbulence.

### 6. FREQUENCY VARIABILITY

The time scale of diffractive scintillation for PSR J1824–2452A at  $\sim 1400$  MHz is  $\Delta t_d \sim 100$  s (Cognard et al. 1996). The corresponding frequency scale is given by  $\Delta \nu_d = 1/2\pi\tau_b$  (Rickett 1996). Here  $\tau_b \sim 2.5 \mu\text{s}$  is the scattering timescale, so  $\Delta \nu_d \sim 0.1$  MHz. Both  $\Delta t_d$  and  $\Delta \nu_d$  are much smaller than our observation timescales and bandwidths. Little variability is therefore expected in our observations. Breaking the 2003 April observation into 300 s sections confirmed that there was no variability beyond what can be explained by a low signal to noise ratio. In contrast, the GPs vary widely in their spectral characteristics. Frequently pulses observed in one 64 MHz band are not detected at all in the other 64 MHz band. Pulse intensities also tend to drop to below our detection sensitivities within the bands. The top panel of Figure 7 shows two pulses observed 3900 s apart that have nearly inverted frequency dependencies. Pulse B is at least 10 times stronger at 1361 MHz than it is at 1313 MHz. The lower panel shows that the integrated emission in the 300 s window around the pulse only varies by around a factor of  $\sim 2$  across the band. The variability seen in the upper panel therefore cannot be due to propagation in the ISM or variability of all emission. It is restricted to the GPs and is therefore probably intrinsic to their emission mechanism.

### 7. DISCUSSION

Our simultaneous observations of GPs at 2700 and 3500 MHz show that the GPs are not a narrow-band phenomena. However, the disappearance of the pulses within our 64 MHz bands at 20 cm indicates that detection at any frequency is almost entirely dictated by the narrow-band ( $\lesssim 64$  MHz) frequency characteristics of the pulses. Perhaps then the GPs are composed of finely spaced nano-pulses that have narrow bandwidths? If each such nano-pulse peaks at a different frequency, the GPs could vary in strength over small bandwidths, but be detectable over large bandwidths. A similar phenomenon occurs for the Crab pulsar (Eilek et al. 2002; Jessner et al. 2005). Testing this hypothesis requires observations of high time-resolution. These would need to be taken simultaneously over multiple frequency bands so that detection of different nano-pulses at different frequencies could be distinguished from DM errors. Another consequence of narrow-band nano-pulses would be a frequency-dependent position angle. Detection of such an effect would require simultaneous polarimetric observations over multiple frequency bands. Notably, none of the pulses we observed gave a satisfactory RM fit, so our observations do not rule out such a hypothesis.

Our observations at 3500 MHz show GPs from

PSR J1824–2452A that are at most 100 ns wide. The Crab pulsar spins just  $\sim 10$  times slower than PSR J1824–2452A, yet it emits in envelopes that are up to  $\sim 1000$  times broader! This means that envelope width is unlikely to scale as a linear function of period.

Rate of GP emissivity cannot even be moderately dependent on  $B_{LC}$ . This is because PSR J1824–2452A emits a  $20\langle E \rangle$  pulses 4000 times less frequently than the Crab pulsar, despite its  $B_{LC}$  being 80% that of the Crab pulsar (Knight et al. 2006). The Crab pulsar has a spin-down luminosity  $\sim 200$  times larger than PSR J1824–2452A, so although  $\dot{E}$  seems a better determinant of GP emissivity than  $B_{LC}$ , it alone cannot account for the  $\sim 4000$  factor in the emissivity rates. We found that the GPs from PSR J1824–2452A occur at pulse phases where the integrated emission has the steepest spectra. Perhaps then this is a factor? In the model of GP emission of Petrova (2004), photons are Compton scattered from low frequencies to high frequencies. Pulsars with steep spectra therefore have the largest capacities for amplification, and so GPs should be seen most readily for steep-spectrum sources. This is indeed what is seen — the millisecond pulsars that emit GPs all have steep spectra (Knight et al. 2006). However, the correlation is by no means compelling — further detections of emitters are needed to help determine if  $\alpha_{\text{spec}}$  really contributes to emissivity.

All GP components of millisecond pulsars appear to have associated X-ray components and vice-versa. The simplest interpretation of this is that GP emission originates in the same part of the magnetosphere as the X-ray emission, albeit at a narrower range of altitudes. Alternatively, any theory wherein GPs are produced in similar parts of the magnetosphere as ordinary emission must explain their disparate polarization properties, and how the narrow emission window of PSR J1824–2452A is shifted to a phase where X-ray emission peaks.

## 8. CONCLUSIONS

We have performed baseband searches for microsecond bursts of emission from sources in the globular cluster M28. We detected 25 pulses at 20 cm and 2 pulses at both 2700 and 3500 MHz, all from PSR J1824–2452A. The emission rate of these giant pulses relative to the emission of ordinary pulses is approximately half that of PSR B1937+21. The pulses occur in two narrow regions of phase that coincide with the X-ray peaks, but occur on the trailing edges of the radio components. At 2700 MHz individual pulses were detected at phases where the corresponding component of the integrated emission was too weak to detect. The integrated radio emission in the main emission regions has a very steep spectrum of up to  $\alpha_{\text{spec}} \sim -4.4$ . The X-rays are emitted over a wider phase range than the giant pulses, so the two emission phenomena likely originate from similar regions in the magnetosphere but may not originate from the same physical mechanism.

The giant pulses have polarimetric properties that are completely different to those of ordinary emission. The integrated emission has no discernable circular polarization, but the giant pulses are up to 60% circularly polarized. Their linear polarization seems to have no preferred orientation, and a variety of position angles are observed. This could mean that the magnetic field in the emission

regions is variable and overwhelms the dipole field of the pulsar. Some pulses are 100% elliptically polarized; the average polarization fraction being 79%.

The two pulses observed at 3500 MHz have different widths and this may be interpreted as being due to resolution of the envelopes of nano-pulses. Alternatively, the emission volumes may differ. One of the pulses is resolved to be 20 ns wide. The strongest pulse seen at 2700 MHz had an inferred brightness temperature at maximum of  $5 \times 10^{37}$  K. Although individual pulses are seen over 800 MHz of bandwidth, within 64 MHz bands at 20 cm the intrinsic pulse-intensity fluctuates significantly. This indicates that the giant pulses could consist of nano-pulses that are individually narrow band.

Parkes Observatory is funded by the Commonwealth of Australia for operation as a National Facility managed by CSIRO. The staff of Parkes Observatory are thanked for their assistance in helping us obtain the data used in this paper. We thank A. Hotan, W. van Straten, and C. West for observing and computing assistance. We thank A. Rots for providing high energy data. HSK acknowledges the support of a CSIRO Postgraduate Student Research Scholarship.

## REFERENCES

- Backer, D. C. & Sallmen, S. 1997, *AJ*, 114, 1539
- Bailes, M. 2003, in *Radio Pulsars*, ed. M. Bailes, D. J. Nice, & S. Thorsett (San Francisco: Astronomical Society of the Pacific), 57–64
- Cognard, I. & Backer, D. C. 2004, *ApJ*, 612, L125
- Cognard, I., Bourgois, G., Lestrade, J.-F., Biraud, F., Aubry, D., Darchy, B., & Drouhin, J.-P. 1996, *A&A*, 311, 179
- Cognard, I., Shrauner, J. A., Taylor, J. H., & Thorsett, S. E. 1996, *ApJ*, 457, L81
- Edwards, R. T. 2001, PhD thesis, Swinburne University of Technology
- Eilek, J. A., Arendt, P. N., Hankins, T. H., & Weatherall, J. C. 2002, in *Neutron Stars, Pulsars, and Supernova Remnants*, ed. W. Becker, H. Lesch, & J. Trümper, 249
- Foster, R. S., Fairhead, L., & Backer, D. C. 1991, *ApJ*, 378, 687
- Hankins, T. H., Kern, J. S., Weatherall, J. C., & Eilek, J. A. 2003, *Nature*, 422, 141
- Hankins, T. H. & Rickett, B. J. 1975, in *Methods in Computational Physics Volume 14 — Radio Astronomy* (New York: Academic Press), 55–129
- Harris, W. E. 1996, *AJ*, 112, 1487
- Hotan, A. W., van Straten, W., & Manchester, R. N. 2004, *PASA*, 21, 302
- Jessner, A., Slowikowska, A., Klein, B., Lesch, H., Jaroschek, C. H., Kanbach, G., & Hankins, T. H. 2005, *Adv. Space Res.*, 35, 1166
- Kinkhabwala, A. & Thorsett, S. E. 2000, *ApJ*, 535, 365
- Knight, H. S. 2006, *Chin. J. Astron. Astrophys.*, submitted
- Knight, H. S., Bailes, M., Manchester, R. N., & Ord, S. M. 2005, *ApJ*, 625, 951
- Knight, H. S., Bailes, M., Manchester, R. N., Ord, S. M., & Jacoby, B. A. 2006, *ApJ*, 640, 941
- Lundgren, S. C., Cordes, J. M., Ulmer, M., Matz, S. M., Lomatch, S., Foster, R. S., & Hankins, T. 1995, *ApJ*, 453, 433
- Lyne, A. G., Brinklow, A., Middleditch, J., Kulkarni, S. R., Backer, D. C., & Clifton, T. R. 1987, *Nature*, 328, 399
- Ord, S. M., van Straten, W., Hotan, A. W., & Bailes, M. 2004, *MNRAS*, 352, 804
- Petrova, S. A. 2004, *A&A*, 424, 227
- Popov, M., Soglasnov, V., Kondrat'ev, V., Kostyuk, S., Ilyasov, Y., & Oreshko, V. 2006, *Astronomy Letters*, 50, 55
- Popov, M. V., Soglasnov, V. A., Kondrat'ev, V. I., & Kostyuk, S. V. 2004, *Astronomy Letters*, 30, 95
- Rand, R. J. & Lyne, A. G. 1994, *MNRAS*, 268, 497
- Ransom, S. M., Hessels, J. W. T., Stairs, I. H., Freire, P. C. C., Kaspi, V. M., & Camilo, F. 2005, *American Astronomical Society Meeting Abstracts*, 207
- Rickett, B. 1996, in *ASP Conf. Ser. 105: IAU Colloq. 160: Pulsars: Problems and Progress*, ed. S. Johnston, M. A. Walker, & M. Bailes, 439–446
- Romani, R. & Johnston, S. 2001, *ApJ*, 557, L93
- Rots, A. H., Jahoda, K., Macomb, D. J., Kawai, N., Saito, Y., Kaspi, V. M., Lyne, A. G., Manchester, R. N., Backer, D. C., Somer, A. L., Marsden, D., & Rothschild, R. E. 1998, *ApJ*, 501, 749
- Saito, Y., Kawai, N., Rots, A., Kamae, T., & Shibata, S. 2001, in *ASP Conf. Ser. 251: New Century of X-ray Astronomy*, ed. H. Inoue & H. Kunieda, 404
- Sallmen, S., Backer, D. C., Hankins, T. H., Moffett, D., & Lundgren, S. 1999, *ApJ*, 517, 460
- Soglasnov, V. A., Popov, M. V., Bartel, N., Cannon, W., Novikov, A. Y., Kondratiev, V. I., & Altunin, V. I. 2004, *ApJ*, 616, 439
- Staelin, D. H. & Reifenstein, III, E. C. 1968, *Science*, 162, 1481
- Stairs, I. H. 1998, PhD thesis, Princeton University
- Stairs, I. H., Thorsett, S. E., & Camilo, F. 1999, *ApJS*, 123, 627
- van Straten, W. 2003, PhD thesis, Swinburne University of Technology

TABLE 1  
SEARCH PARAMETERS.

Date (1)	Receiver (2)	$\nu$ (MHz) (3)	SEFD (Jy) (4)	$T_1$ (s) (5)	$T_2$ (s) (6)	$S_A$ (mJy) (7)	$E_{\text{lim}}$ (Jy $\mu$ s) (8)	$E_{\text{lim}}$ ( $\langle E \rangle_A$ ) (9)
2003 February 10	Multibeam	1341	39	6700	320	2.7	91	11
		1405	38	6700	490	1.7	89	18
2003 April 15	H-OH	1341	49	7700	1200	2.6	113	14
		1720	46	7700	1300	1.6	105	22
2003 December 14	10 cm feed of 10/50 coaxial	2700	45	9200	730	0.20	103	170
		3500	45	9200	760	0.12	103	280
2004 November 11	Multibeam	1341	39	2800	220	1.8	91	17
2004 December 12	Multibeam	1405	38	670	17	4.4	89	7

TABLE 2  
 FRACTIONAL POLARIZATIONS OF GIANT PULSES.

Polarization Type	Min	Mean	Max
(1)	(2)	(3)	(4)
Circular	0.0	0.27	0.6
Linear	0.4	0.73	1
Total	0.4	0.79	1
Ratio of circular to linear	0.0	0.36	0.8



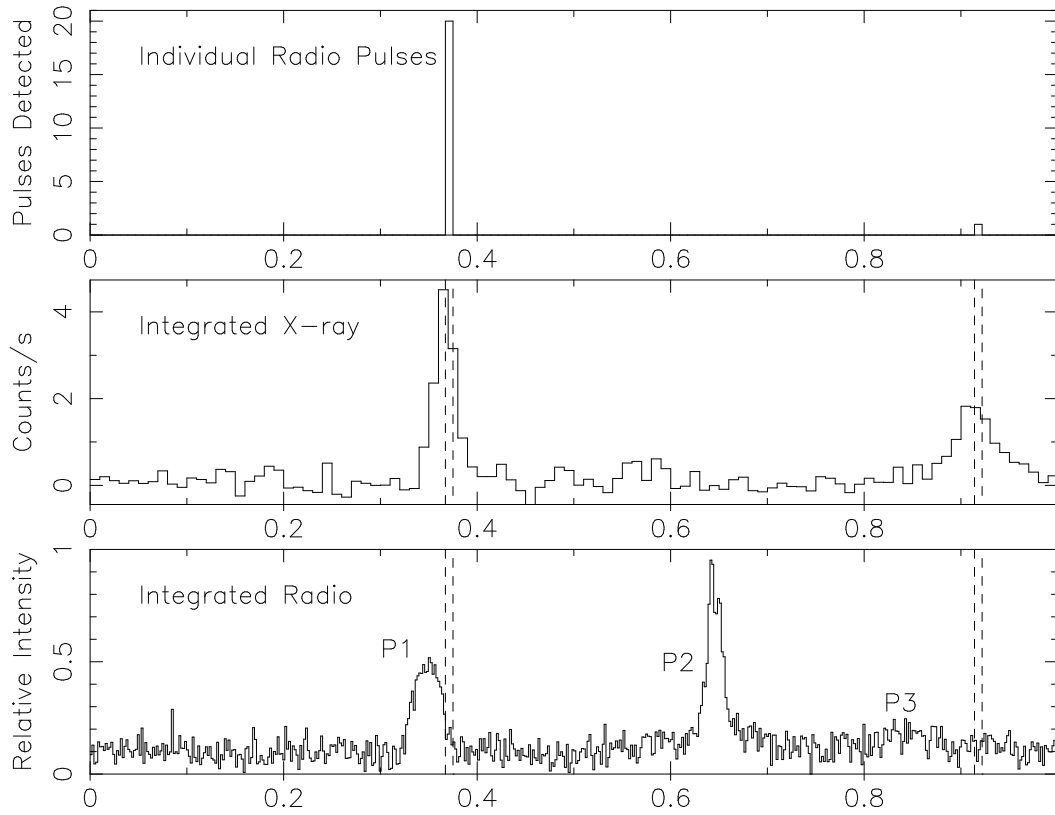


FIG. 1.— Relative phases of emission from PSR J1824–2452A. (a) Phases of giant pulses detected in 2003 February and 2003 April. (b) The RXTE 2 – 16 keV pulse profile of PSR J1824–2452A reproduced from Saito et al. (2001). Phase alignment was performed by noting that in the data of Rots et al. (1998) the peak of the X-ray profile trails the leading radio-pulse by 0.017 pulse periods. The X-ray phases are accurate to around  $10 \mu\text{s}$ . Rots et al. determined this alignment using the radio ephemerides of Backer & Sallmen (1997). (c) Mean pulse profile at 1341 MHz created from 2003 April data.

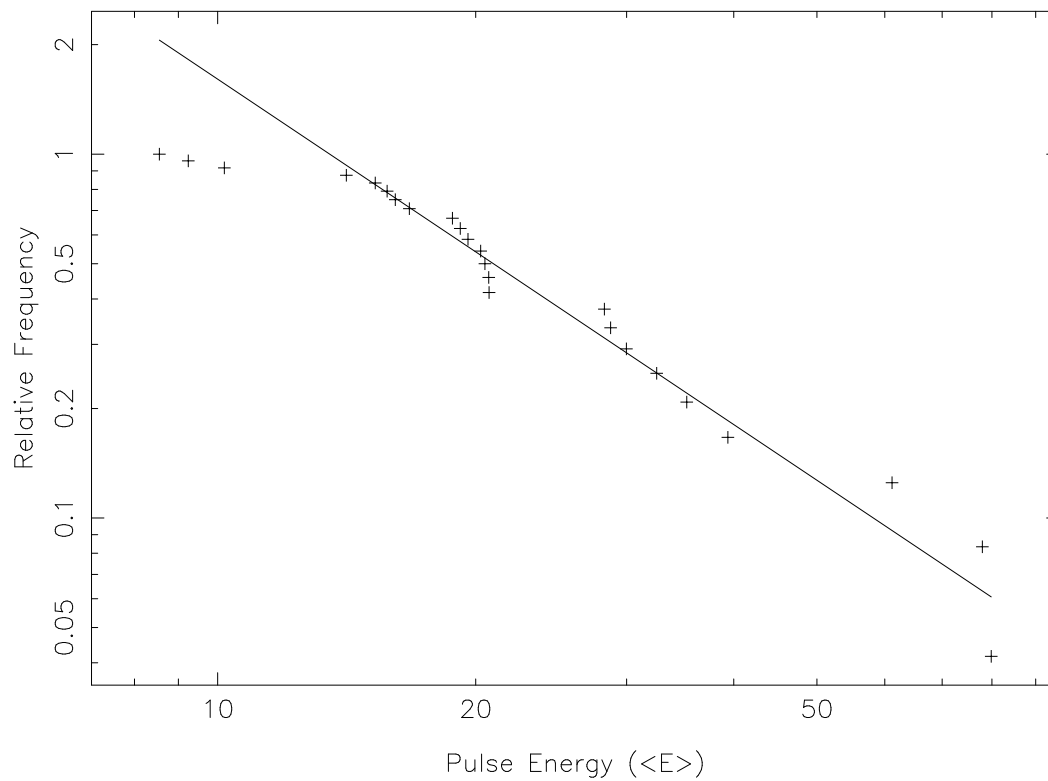


FIG. 2.— Cumulative probability distribution of 20 cm pulse energies. The solid line denotes the line of best fit, excluding the 3 pulses with the lowest energies, and the 3 pulses with the highest energies. It has a slope of  $-1.6$ .

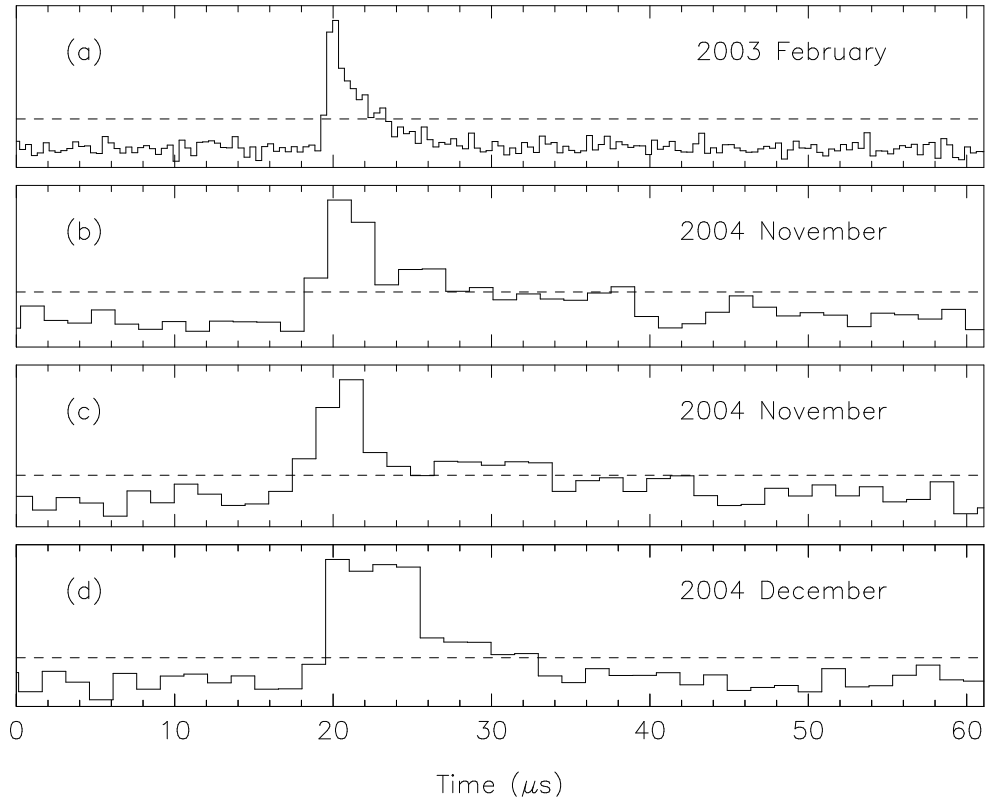


FIG. 3.— Variable scattering timescales between 2003 and 2004. (a): Pulse observed in 2003 February at 1341 MHz. (b) and (c): Pulses observed in 2004 November at 1341 MHz. (d): Pulse observed in 2004 December at 1405 MHz. The dashed line indicates 30% of the peak intensity.

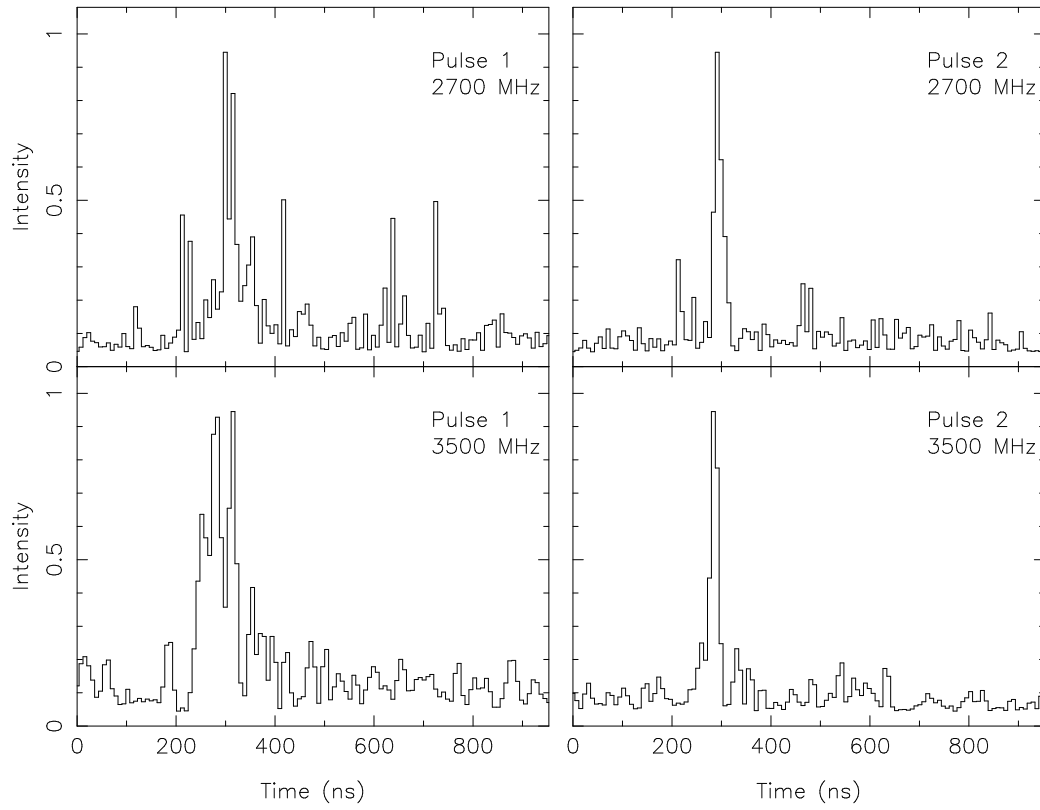


FIG. 4.— Pulses observed at 2700 and 3500 MHz in 2003 December shown at a time resolution of 7.8125 ns.

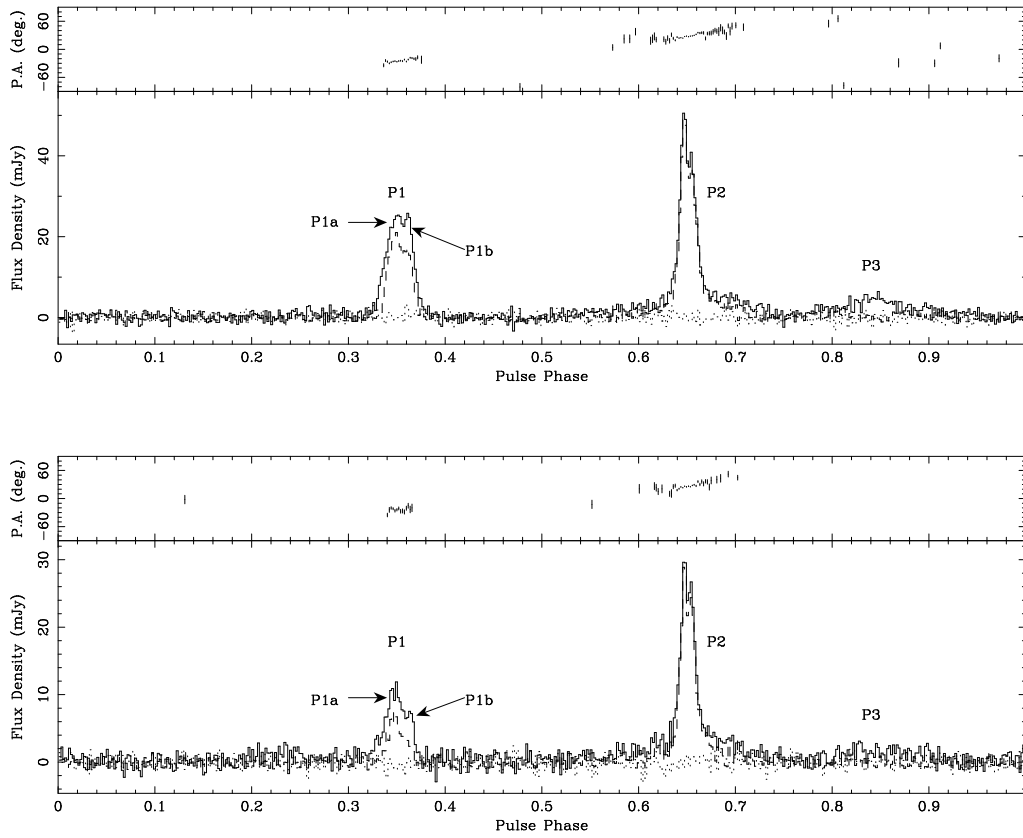


FIG. 5.— Polarization plots of 2003 April observations of PSR J1824–2452A at 1341 MHz (top) and 1720 MHz (bottom). The solid, dashed, and dotted lines denote total, linearly polarized, and circularly polarized emission respectively. The position angle corrected for Faraday rotation is shown at the top of each profile. The position angles shown are not absolute.

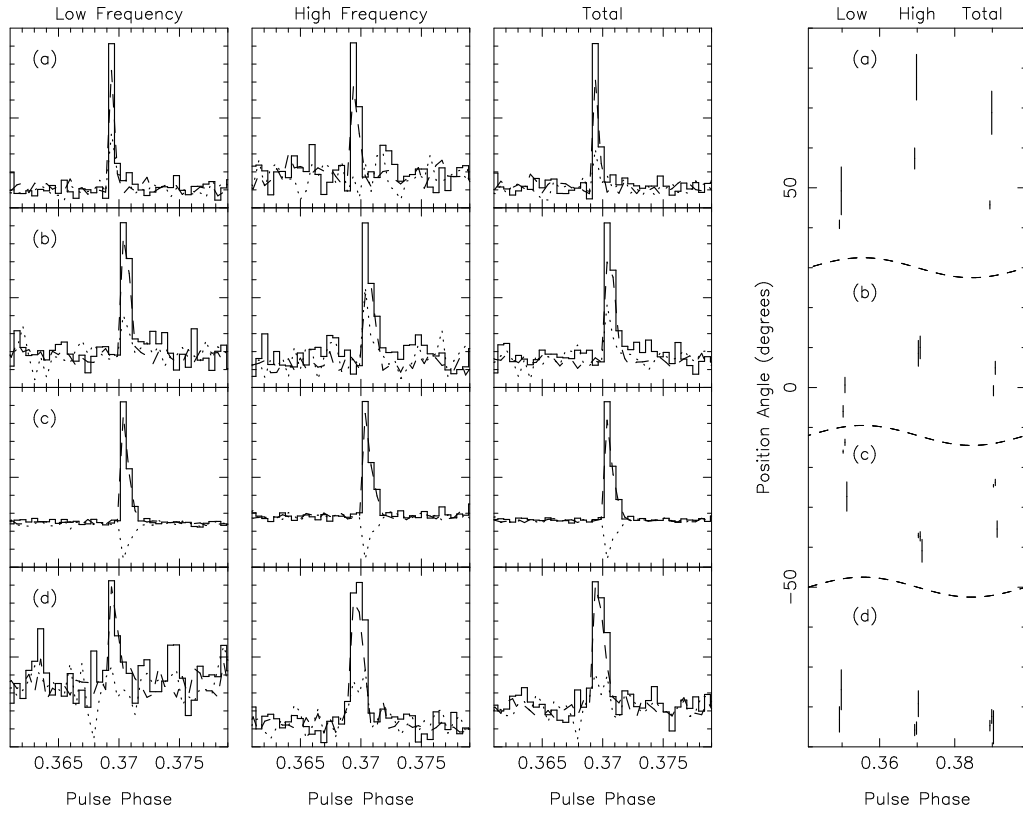


FIG. 6.— Polarization plots and position angles of four strong GPs observed at 20 cm. The left three columns show polarization plots of the GPs. The first two columns respectively show the polarization of each GP in the low-frequency and high-frequency halves of the observing band. The third column shows the polarization of each GP over the full band. Total intensity, linear polarization, and circular polarization are shown by solid, dashed, and dotted lines respectively. The fourth column shows the position angles of these pulses — each of sections (a)-(d) contains only position angles of the corresponding GP. For clarity the phases of the low-frequency and total position angles have been shifted by 0.02 pulse periods to earlier and later phases respectively. The GPs clearly have different position angles to each other. However, the position angle of each pulse is similar for each independent frequency band. Noise cannot explain this consistency, so the position angles shown are intrinsic to the pulses. The position angles are spread over all possible values, so it can be concluded that the emission mechanism of the GPs produces randomly distributed position angles.

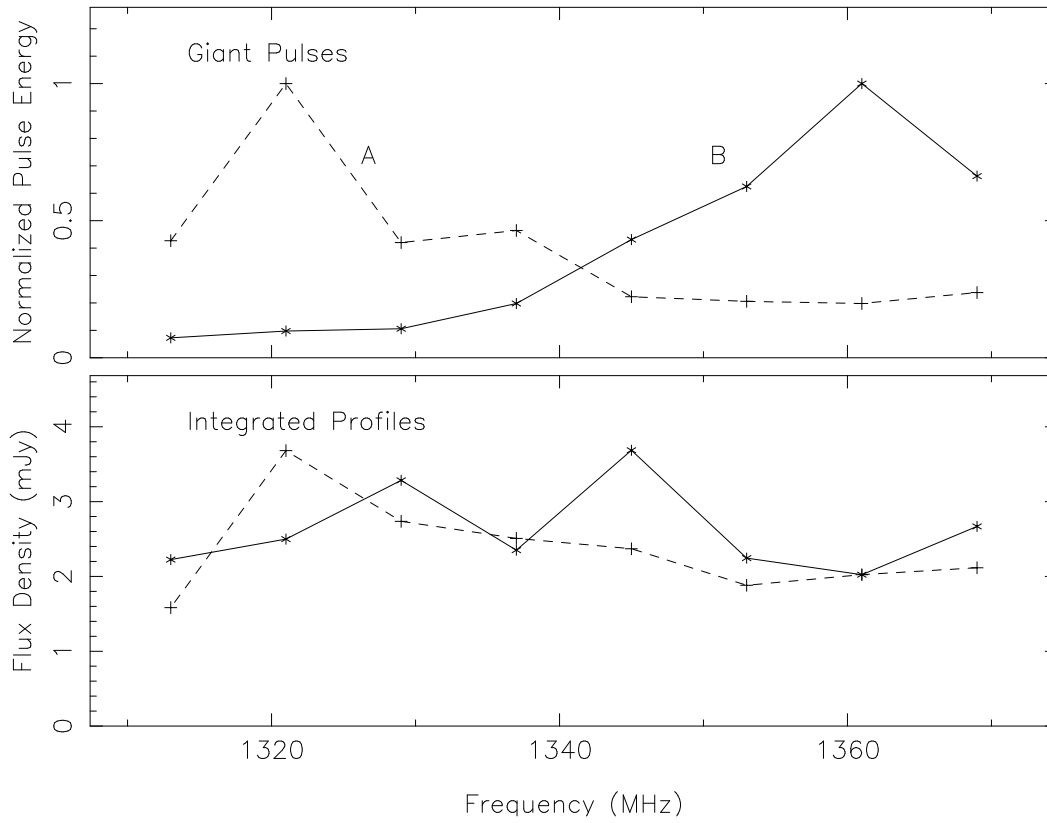


FIG. 7.— Frequency variability of two pulses observed in 2003 April. Top: Spectra of pulse A (dotted line and plus symbols) and pulse B (solid line and asterisks). The energies for frequencies above 1340 MHz (below 1330 MHz) for pulse A (pulse B) are upper limits only. Bottom: Integrated flux-densities for 300 s of data about pulse A (dotted line and plus symbols) and pulse B (solid line and asterisks).